Calixarene-based porous 3D polymers and copolymers with high capacity and binding energy for CO2, CH4 and Xe capture

Journal of
Materials Chemistry A

Materials for energy and sustainability

Accepted Manuscript

This article can be cited before page numbers have been issued, to do this please use: A. Comotti, A. Pedrini, J. PEREGO, S. Bracco, C. Bezuidenhout and P. Sozzani, *J. Mater. Chem. A*, 2021, DOI: 10.1039/D1TA05930K.

ROYAL SOCIETY OF CHEMISTRY

rsc.li/materials-a

View Article Online
DOI: 10.1039/D1TA05930K

ARTICLE

Calixarene-based Porous 3D Polymers and Copolymers with High Capacity and Binding Energy for CO_2, CH_4 and Xe Capture

Received 00th January 20xx,
Accepted 00th January 20xx

DOI: 10.1039/x0xx00000x

Alessandro Pedrini, Jacopo Perego, Silvia Bracco, Charl X. Bezuidenhout, Piero Sozzani and Angiolina Comotti*

The supramolecular capacity of calixarenes towards guests is largely consolidated: on the contrary, the synthesis of porous calixarene-based frameworks by covalent bond formation is still a challenge. Our target was to yield 3D polymers and copolymers based on calixarenes for selective gas-capture, endowed with easy pore accessibility, specific sites and built by a straightforward synthetic route. The covalent calixarene frameworks (CXFs) were prepared by Yamamoto coupling reaction starting from tetrabromo calixarene propoxy- and methoxy-monomers of three stable calixarene (partial cone, effective cone, and 1,3-alternate) conformers and complete post-synthetic deprotection to achieve polar phenolic calixarene derivatives. Moreover, the copolymer of calixarene-based monomers with tetrabromo-tetraphenylmethane exhibited remarkable surface areas up to about 3000 m^2/g. Smart architectures endowed with hierarchical porosity from micro- to meso-porosity showed notable sponge-like swellability by CO_2, which was captured effectively at room temperature, even in competition with N_2, yielding CO_2 removal in column breakthrough experiments. Indeed, CXFs displayed excellent CO_2 and CH_4 energy binding of 35 and 24 kJ/mol, respectively. Ultramicropore sites were highlighted by Xe capture and *in-situ* detection after a few milliseconds xenon diffusion time, by laser-assisted hyperpolarized ^{129}Xe NMR, probing calixarene capsules accessibility and the available space. This synthetic route demonstrated the possibility to modulate at will pore capacity and selectivity, displaying porous frameworks with two distinct pore families, wherein calixarene moieties play the role of small and selective sites. A contractile behavior of the frameworks was observed upon deprotection which produced more polar sites, due to the formation of hydrogen bond networks.

Introduction

Calixarenes (CXs) have been widely applied as supramolecular building-blocks for engineering cavities of various sizes and simultaneous presence of distinct hydrophobic and hydrophilic regions.[1] The cage-like nature of these macrocycles promotes the formation of porous molecular crystals,[2,3] endowed with the so called 0D porosity.[4] Calixarenes are ideal molecular receptors for selective complexation, sensing and gas adsorption at high and low pressure: e.g. crystalline *p-tert*-butylcalix[4]arene has been employed for the absorption of several vapors and gases of energetic relevance and environmental concerns, such as CH_4 and CO_2.[5-8] However, the use of molecular assemblies of calixarene suffer from some limitations with respect to pore tunability and thermal robustness since soft intermolecular interactions are hardly governable to form stable and open pores. On the contrary, these properties are generally associated with Porous Organic Polymers (POPs) or Frameworks (POFs).[9,10] Such architectures offer the opportunity to incorporate macrocyclic moieties with preorganized cavities opening up the perspective to form functional porous materials, containing two hierarchical levels of porosity, due to both the macrocycle specific activity and the framework large pore architecture.[11-14] The approach of exploiting macrocycles or cages inserted as active struts in a robust building for their host-guest key-in-the-lock activity has been explored in cyclodextrin-, pillar[n]arene- and resorcinarene-based POPs which have promised interesting applications especially for iodine sorption, light hydrocarbon and CO_2/N_2 separation. [13-17]

To date, a general strategy of using calixarene macrocycles as struts for the fabrication of porous frameworks capable of adsorbing and separating relevant gases for environmental and industrial applications is still an open issue. This was achieved via the facile Yamamoto cross-coupling reaction of tetrafunctional calixarene monomers and tetrafunctional co-monomers. To our knowledge, only porous frameworks from difunctional ethynyl linkers bridging calixarene moieties by Sonogashira reaction have been realized, whose applications were mainly focused on iodine adsorption and water purification.[18-20]

Herein, we report on the preparation of a new class of covalent calix[4]arene-based frameworks (CXFs) showing outstanding adsorption properties towards CO_2 and CH_4, while selectively

[a] *Department of Materials Science, University of Milano Bicocca, Via R. Cozzi 55, 20125 Milan, Italy.*
[b] *† Footnotes relating to the title and/or authors should appear here.*
Electronic Supplementary Information (ESI) available: [details of any supplementary information available should be included here]. See DOI: 10.1039/x0xx00000x

View Article Online DOI: 10.1039/D1TA09370H

excluding nitrogen. Our synthetic strategy was the use of alkylated calix[4]arene with a precise and controlled conformation which successfully reacted forming the covalent frameworks. After post-synthetic dealkylation, we succeeded in obtaining porous calixarene frameworks and copolymers with easily available hydroxy groups, which increment the interactions of the functionalized host framework with the target gases. Additionally, the conformational flexibility of calixarenes forming partial cone, effective cone, and 1,3-alternate conformations was explored for controlling the spatial organization (topology) of bromine reactive groups towards the Yamamoto reaction and the resulting porosity of the materials. Copolymers were obtained with the participation of a second tetrafunctional monomer, thus realizing a very effective co-condensation in any stoichiometric proportion to yield customized products. Indeed, copolymers benefited from pore expansion capability of tetraphenylmethane comonomer, achieving the high surface area of 3000 m^2/g. Also, remarkable site-affinity *vs* xenon was shown at high sensitivity with 2% diluted Xe gas in He and N_2 mixtures, by *in-situ* laser-assisted hyperpolarized ^{129}Xe NMR, which reported on fast accessibility of calixarene receptors through the open framework and provided the description of the confining sites. The frameworks exhibited optimal binding for CH_4 storage and high CO_2 selectivity in a CO_2/N_2 mixture from a flue gas in operative conditions as demonstrated by breakthrough experiments.

Results and discussion

Calix[n]arenes show several advantages as molecular receptors, including their synthetic versatility and conformational tunability. Even-numbered calix[n]arenes (n = 4, 6, 8) are commercially available, and they can be easily obtained on the kilogram scale by the condensation under basic conditions[21] of cheap reagents (phenols and formaldehyde), by well consolidated synthetic procedures.[22] Moreover, calix[n]arenes are extremely versatile molecular scaffolds which exhibit a dual property due to their flexible conformation: in fact, they are able to form induced-fit binding and finely preorganize their structure in a proper locked conformation. In the case of the calix[4]arene, non-alkylated and tetramethoxy derivatives are conformationally flexible, forming a macrocycle into one of the four accessible conformations, at room temperature namely *full-cone*, *partial cone*, *1,2-and 1,3-alternate* conformers.[23]

We envisaged the control of the macrocyclic monomer structure as a powerful tool for the spatial preorganization of the reactive groups during the formation of the porous covalent framework. In particular, we synthesized three alkylated calix[4]arenes **CX1**-**CX3**, bearing four bromine substituents in *para* positions suitable for Yamamoto-type Ullmann coupling reaction to build porous networks (Figure 1). In our design, the different spatial orientation of the bromine atoms can affect the network growth in the three directions, thus leading to materials having different porosities. The three monomers were prepared in two steps from commercially available 25,26,27,28-tetrahydroxycalix[4]arene by modified previously reported procedures (see ESI for the detailed synthetic procedures). In the first step, calix[4]arene phenols were alkylated following stereoselective procedures to afford tetraalkylated compounds, which were subsequently brominated in *para* position with *N*-bromosuccinimide. Alkylated tetrabromo-calix[4]arenes **CX1**-**CX3** were obtained in good purity by recrystallization and were fully characterized by 1D and 2D NMR spectroscopy (Figures S1-S13). The partial cone, 1,3-alternate and full-cone conformations in solution of **CX1**, **CX2** and **CX3,** respectively, were clearly determined by the analysis of the pattern of the methylene protons signals in ^1H NMR spectra.[24] Tetrabromo-calix[4]arenes **CX1** and **CX2** were then homopolymerized by Yamamoto-type coupling reaction to afford frameworks denoted **CXF1-OMe** and **CXF2-OPr**, respectively (Figure 1).

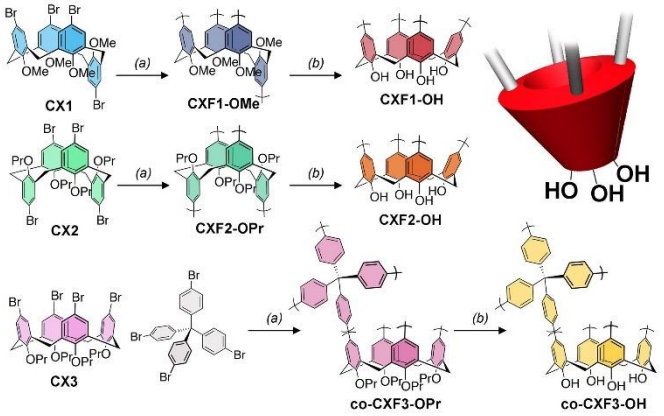

Figure 1. Synthetic scheme for preparation and post-synthetic modification of **CXFs**. Experimental conditions *(a)* $Ni(COD)_2$, *cis*,*cis*-1,5-cyclooctadiene, 2,2'bypiridyl in DMF/THF 3:1 at RT for 48 h for cross-coupling reaction; *(b)* BBr_3 at RT for 24 h for dealkylation.

Additionally, copolymerization of **CX3** monomer and tetrakis(4-bromophenyl)methane, precursor of high surface area porous aromatic frameworks (PAFs)[25] to yield a copolymer wherein calix[4]arene moieties are integrated in a common framework. Yamamoto cross-coupling reaction allowed for the formation of a network of carbon bonds between bromine-functionalized aromatic groups on the comonomers (Figure 1). In order to further enhance the effect of the presence of polar groups in the framework, the phenoxy groups of calixarene scaffolds were post-synthetically transformed into phenol groups. **CXF1-OMe**, **CXF2-OPr** and **co-CXF3-OPr** were post-synthetically deprotected with an excess of boron tribromide to obtain the corresponding framework decorated with free hydroxy groups, affording **CXF1-OH**, **CXF2-OH** and and **co-CXF3-OH** as tan and off-white powders, respectively (Figure 1).

The **CXF1-OMe**, **CXF2-OPr** and **co-CXF3-OPr** solids, insoluble in all common solvents, were characterized by FTIR spectroscopy which showed diagnostic signals of each monomer unit (Figure S14,S15).[26] No long-range periodic order was observed in the powder X-ray diffraction patterns indicating the amorphous nature of these materials (Figure S16,S17). TGA analyses exhibited a high thermal stability, as a consequence of the fully covalent nature of the networks (Figure S18,S19): the frameworks degrade above 500°C in

the air except for **CXF1-OMe** wherein the methoxy groups decompose at 300°C.

Magic angle spinning (MAS) ^{13}C NMR spectra show the chemical structure of the frameworks and the conformations of calixarene moieties (Figure 2). Signal assignments were established by comparison to solution ^{13}C NMR spectra of the monomers (Table S1,S2). In ^{13}C MAS NMR spectrum of **CXF1-OMe** sample, characteristic signals due to the condensation reaction of calixarene moieties appear in the aromatic region, in particular the peak at δ = 137.4 ppm of C_4 is diagnostic for the formation of the framework (Figure 2a). The signal due to residual C-Br, which is expected to resonate at about δ = 115 ppm, is absent. Additionally, a resonance at δ = 60.2 ppm was detected, demonstrating the presence of the methoxy groups. Interestingly, the two distinct signals at δ = 31.2 and 37.9 ppm in the methylene region are in agreement with the preservation of the partial cone conformation which implies two signals of 1:1 intensity ratio, as detected in the spectrum. The effective removal of alkoxy groups was shown by ^{1}H and ^{13}C MAS NMR (Figure 2b). After dealkylation, the $^{13}C\{^{1}H\}$ MAS spectra of **CXF1-OH** shows the almost complete disappearance of the signal at δ = 60.2 ppm (residual peak below 3%), showing the formation of polycalix[4]arene phenol. Moreover, the aromatic resonance at δ = 151.3 ppm assigned to the C_{arom}-OH (C_1) undergoes an upfield shift of $\Delta\delta$ = 5.9 ppm from the pristine sample. Interestingly, the notable change of the ratio between the signals of methylene bridges 5 and 5' (from 1:1 to 5:1) suggests a reorganization in favour of the more stable *full-cone* conformation, which is driven by the maximization of hydrogen bonding interactions. A similar behaviour was observed for **CXF2-OPr** which exhibits the full dealkylation to **CXF2-OH** and conversion (4:1) to the *full-cone* conformation (Figure S20). Thus, the framework swelling, promoted by adsorption of the dealkylation solvent, allows further degrees of freedom and the relaxation of calixarene units to lower energy conformation, even in the presence of constrains in the covalent frameworks. The removal of alkoxy groups was confirmed by the appearance of an infrared band at wavenumbers between 3000-3500 cm^{-1} in the IR spectrum (Figure S15). To our knowledge, these are the first porous frameworks of homopolymer made purely by phenol-based calixarene monomeric units.

In **co-CXF3-OPr**, besides the signals of calixarene moieties, typical signals of the presence of atoms on *p*-phenylene rings appear in the aromatic region (Figure 2c, highlighted green). The peak at δ = 64.7 ppm (C_9) belongs to the central quaternary carbon atom of the tetraphenylmethane units, while the resonances at δ = 77.1, 23.6 and 8.9 ppm correspond to the propoxy groups (C_{11}, C_{12} and C_{13}, respectively). A single resonance at δ = 31.2 ppm (C_{10}) is observed for the methylene group of calixarene moiety, indicating the persistence of the cone conformation from the monomer to the copolymer. The framework deprotection is quantitative also in the case of the copolymer as shown by the disappearance of the alkoxy signals (Figure 2d).

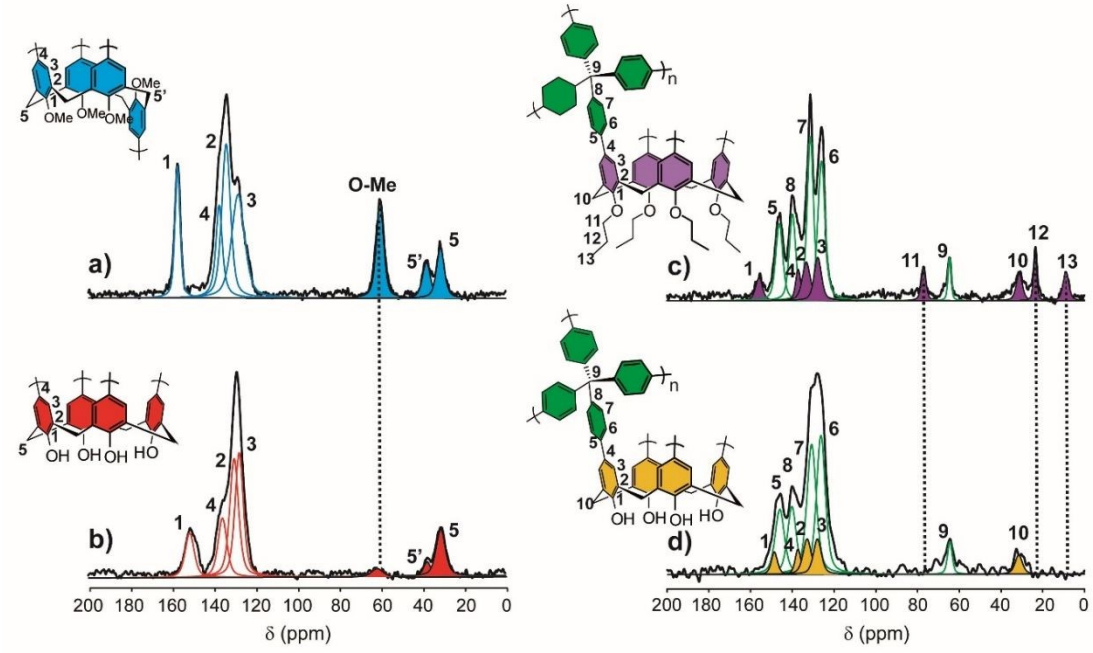

Figure 2. $^{13}C\{^{1}H\}$ MAS NMR spectra of (a) **CXF1-OMe**, (b) **CXF1-OH,** (c) **co-CXF3-OPr** and (d) **co-CXF3-OH** with deconvoluted peaks. A recycle delay of 100 s was applied.

N_2 77 K, CO_2 273 K adsorption isotherms and HP ^{129}Xe NMR. The porosity of the frameworks was evaluated by N_2 adsorption/desorption isotherms at 77 K (Figure 3). The main parameters derived from the isotherms are reported in Table 1. The differential bulkiness of alkoxy substituents slightly affects the performances of **CXF1-OMe** and **CXF2-OPr**, in fact they exhibit

Langmuir surface areas of 687 and 638 m^2/g and Brunauer–Emmett–Teller (BET) surface areas of 626 and 562 m^2/g, respectively. Interestingly, removal of methoxy groups to yield **CXF1-OH** (increased total free volume from 0.29 to 0.32 $cm^3 g^{-1}$) showed the larger contribution of mesopores than its progenitor. Pore-size distribution (PSD) in the micropore region could be better described by the more penetrant CO_2 gas at 273 K: indeed, Non-Local Density Functional Theory (NL-DFT) applying carbon slit pore model, displayed the emergence in the OH-rich framework of the intense peak due to 9 Å pores (absent in the precursor), suggesting the generation of polar small pores that quadrupolar CO_2 explores efficiently (Figure 3c). Another attractive feature of the novel porous calix[4]arene homopolymers is their pore expandability: they undergo swelling upon gas condensation, as evidenced by a large hysteresis loop in the adsorption-desorption profiles of isotherms. This behaviour reflects the framework flexibility promoted by rotational freedom around the single bonds that connect the aromatic units and the conformational flexibility intrinsic to the calixarene units. The adsorption and desorption branches can be reversibly reproduced without reducing the sorption capacity.

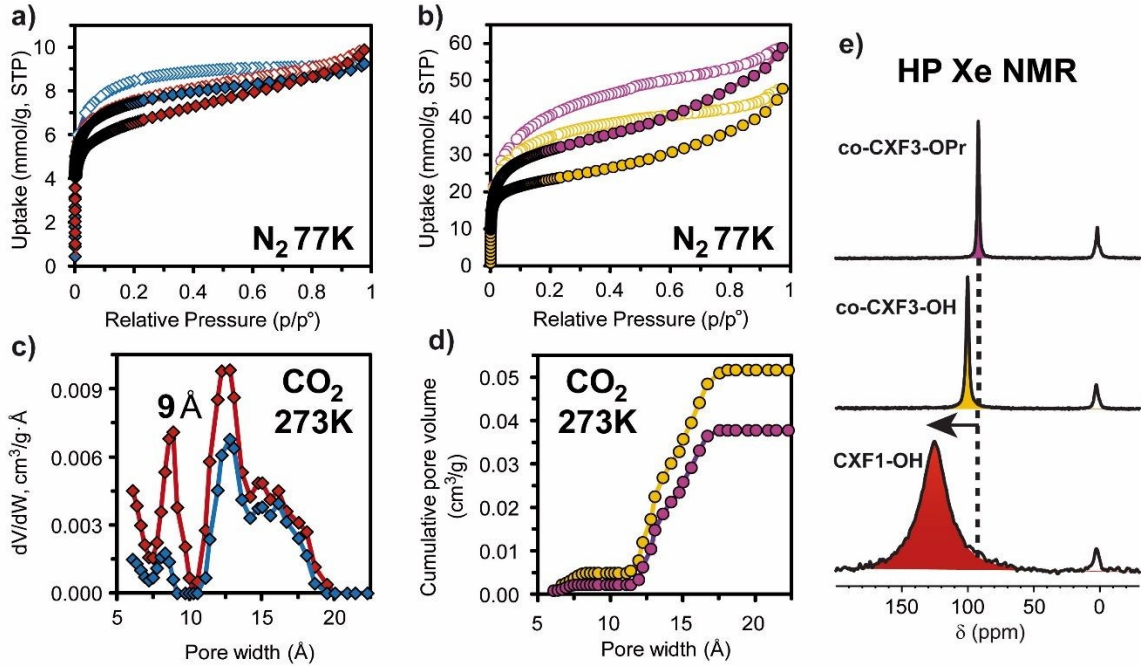

Figure 3. N_2 adsorption isotherms collected at 77 K and up to 1 bar (empty symbols define the desorption branch) of a) **CXF1-OMe** and **CXF1-OH** (blue and red diamonds, respectively); b) **co-CXF3-OPr** and **co-CXF3-OH** (violet and yellow circles). c) Pore size distribution from CO_2 isotherms at 273 K of **CXF1-OMe** and **CXF1-OH** (blue and red diamonds, respectively). d) Cumulative pore volume of **co-CXF3-OPr** and the **OH** analogue (violet and yellow circles, respectively). e) HP ^{129}Xe NMR of calixarene based samples collected at room temperature. The signal at 0 ppm corresponds to free Xenon.

Table 1. Textural parameters of **CXFs** as derived from N_2 adsorption isotherms at 77 K.

	S_{Lang}[a] m^2g^{-1}	S_{BET}[a] m^2g^{-1}	V_{total}[b] $cm^3 g^{-1}$	CO_2 uptake wt%	Q_s[c] kJ mol^{-1}
CXF1-OMe	687	626	0.29	6.6	26.0
CXF1-OH	610	540	0.32	9.7	35.0
co-CXF3-OPr	2966	2609	1.91	10.6	23.2
co-CXF3-OH	2191	1943	1.28	12.8	30.0

[a] calculated using adsorption data in p/p° range from 0.015 to 0.1. [b]calculated using Non-Local Density Functional Theory and Carbon Slit Pores model. [c] Q*st* was calculated from CO_2 isotherms at 273 K, 283 K and 298 K. For CXF1-OH Q*st* was calculated from microcalorimetry.

On the opposite, the attempts to synthetise **CXF3-OPr** homopolymer framework was unsuccessful and its porosity was negligible, possibly due to bromine orientation towards the same side of the cone that prevents the 3D network growth. This problem was circumvented by copolymerization together with a second tetrafunctional monomer with tetrahedral symmetry (tetraphenylmethane), which promoted much higher surface areas. Indeed, **co-CXF3-OPr** showed the highest surface area (2966 and 2609 $m^2 g^{-1}$ with Langmuir and BET model, respectively) (Figure 3b). The isotherm highlighted an important contribution of the mesoporosity, that was assessed at about the 50% of the total pore volume. Moreover, N_2 desorption branch runs distinctly above the adsorption curve, forming a hysteresis loop closing only at very low pressures. This finding can be ascribed to both the 3D framework swellability and the conformational flexibility of the newly formed carbon-carbon connecting bonds coupled with the intrinsic softness of

calix[4]arene methylene bridges.[27] After post-synthetic deprotection (**co-CXF3-OH**) a contraction of total pore volume, as observed with N_2 adsorption isotherms: this is the consequence of the restricted polar environment, which makes the framework locally inaccessible to N_2. To discriminate the pore distribution in the micropore region, CO_2 adsorption profile collected at 273K and its pore size distribution showed clearly a 20% increase of the cumulative micropore sorption in **co-CXF3-OH** with a major contribution from 12 to 18 Å (Figure 3d).

Hyperpolarized (HP) ^{129}Xe NMR is a laser-assisted technique which provides a unique tool to report on the size of the cavities immediately after hyperpolarized gas migrated through the open pores to reach the preferred sites. Actually, the exceptional sensitivity allows for a direct report of Xe signal while exploring the confined spaces, manifested by high chemical shift values with respect to the gas phase set at δ = 0 ppm (Figure 3e).[28-31] The copolymer **co-CXF3-OPr** exhibited a sharp peak for the confined gas at a chemical shift as high as δ = 90 ppm, demonstrating in an unconventional fashion the easy accessibility of the calixarene sites, after a few millisecond diffusion-time of the fresh hyperpolarized gas and the availability of the material to Xe diffusion. A further chemical shift increase to δ = 100 ppm from the **co-CXF3-OPr** to the **co-CXF3-OH** was observed, revealing a restriction of explored pores and a greater affinity of Xe with interacting sites, in agreement with microporous nature of the framework as observed from the CO_2 isotherm analysis at 273 K (Figure 3d). The extremely narrow linewidth is an indication for a homogeneous distribution of monomer units, generating a uniform confining environment. The homopolymer **CXF1-OH**, made of solely calixarene units and bearing OH groups, produced a higher chemical shift at δ = 125 ppm (δ = 159 ppm at 239 K), demonstrating the stronger confinement of Xe atoms into the calixarene cavity. This result is in agreement with the appearance of 9 Å pore size, as discussed for CO_2 isotherm (Figure 3c). It is worth noting that the gas mixture flowing into the samples contains only 2% Xe diluted in He/N_2 with a partial pressure of 14 mmHg. The high response of confined Xe with respect to free gas is diagnostic of the selective adsorption of Xe on interacting sites.

CO_2 and CH_4 adsorption, microcalorimetry and breakthrough. Prompted by the performances in N_2 adsorption isotherms, we selected **CXF1-OH** as a suitable candidate for CO_2 and CH_4 capture. CO_2 sorption isotherms were collected at 195 K up to 1 bar and at three different temperatures (273 K, 283 K and 298 K) up to 10 bar (Figure 4 and Figures S30-S32). The uptake up to 1 bar for **CXF1-OH** reaches 1.5 mmol g^{-1} at ambient temperature and 2.2 mmol g^{-1} at 273 K, corresponding to 6.6 wt % and 9.7 wt %, respectively (Figure 4a). These values are comparable to the CO_2 uptake recently reported for *C*-phenylresorcin[4]arene-based porous organic polymers bearing free phenolic functionalities.[17]

Microcalorimetry coupled with adsorption isotherms for simultaneous acquisition of CO_2 adsorption enthalpy and loading[32] yielded an enthalpy value at low coverage (Q_{st}) of 35 kJ mol^{-1} for **CXF1-OH** (Figure 4b and Figures S34-S38), which is remarkably higher than that obtained for **CXF1-OMe** (26 kJ mol^{-1}). The high density of hydroxyl groups favors multiple CO_2 interactions and is responsible for the high enthalpy value. The 35 kJ/mol value is among the highest values achieved in hydroxyl functionalized covalent frameworks[17,33,34] and is considered to be a good balance for efficient delivery cycles.

The prominent difference in the CO_2 uptake with respect to N_2 under the same pressure and temperature conditions prompted us to calculate the CO_2/N_2 selectivity using Ideal Adsorbed Solution Theory (IAST) applied to single-component isotherms starting from a 15:85 (CO_2:N_2) mixture in order to simulate the flue gas conditions (Figure 4c). The CO_2/N_2 selectivity at 273 K exhibited a value of 98 at low pressures (<0.1 bar). This value overcomes the performance of PAF3 (*S*=87 at 273K) and is comparable to NPAF (*S*=98 at 298 K) and PAF33 (*S*=99 at 273K) .[35]

Breakthrough adsorption experiments[36] were performed to test **CXF1-OH** for the separation of N_2 / CO_2 mixtures, using binary gas-mixture streams with gas compositions of 5% and 15% and a flow of 4 cm^3/min. At 298 K and 1 bar, CO_2 was completely removed from the mixture while N_2 was released by the column to a purity of more than 99% for 21 min/g and 16 min/g, respectively, corresponding to 0.19 mmol/g and 0.44 mmol/g retention, in agreement with adsorption isotherms (Figure 4d). After multiple adsorption/desorption cycles with 0.15/0.85 CO_2/N_2 gas mixture, the performance of **CXF1-OH** was unaltered (Figure 4f). The activation of the sample can be easily performed by a flow of inert gas such as N_2 and no thermal treatment was necessary. This is one of the few breakthrough experiments for CO_2/N_2 separation in POPs which could be of interest for industrial applications such as CO_2 capture from flue gas.[37]

Since enhanced interactions can be expected also towards CH_4 owing to the polarity of the PhOH groups, CH_4 adsorption measurements were performed at various temperatures on both **CXF1-OMe** and **CXF1-OH** (Figure 4g and S42,S43). The compound **CXF1-OMe** showed excellent CH_4 binding energy performance, reaching the notable value of 21 kJ mol^{-1} (Figure S45) that exceeds, the performances of common MOFs, such as UTSA-20 (18.2 kJ mol^{-1}), PCN-14 (18.7 kJ mol^{-1}) and HKUST-1 (17 kJ mol^{-1}).[38] Upon dealkylation, the framework reaches the value of 24 kJ mol^{-1}, approaching the value of best performing porous organic frameworks such as lithiated framework TAF-OLi (25 kJ mol^{-1})[34] and COFs (COF-1: 25.1 kJ mol^{-1}).[39] These results are particularly impressive if we take into account the absence of metal ions in our fully organic network. The adsorption energy falls in the ideal range for efficient capture/release cycles: this feature, together with the stability of covalent bonds, makes **CXF1-OH** promising for methane storage and delivery applications.

CO_2 and CH_4 adsorption analyses were performed also on **co-CXF3-OPr** and **co-CXF3-OH** (Figure 4h and Figures S46,S47). Owing to their high surface area, **co-CXF3-OPr** and **co-CXF3-OH**

show a remarkable CO_2 uptake at 195 K and 1 bar, reaching the values of 33 mmol g^{-1} and 29 mmol g^{-1}, respectively, which correspond to 147% and 128% of their weight, respectively. CO_2 adsorption value at 273 K and 1 bar for **co-CXF3-OH** (2.9 mmol g^{-1}) is higher than that measured for **co-CXF3-OPr** (2.4 mmol g^{-1}) (Figure 4h). Anyway, they are superior to that reported for unfunctionalized PAF-1 (2.0 mmol g^{-1}), despite **co-CXF3-OH** has the lowest BET surface area (1943 vs. 4100 m^2 g^{-1} for **co-CXF3-OPr** and PAF-1[25], respectively). CO_2 uptake of **co-CXF3-OH** is even higher than other phenolic hydroxyl-functionalized PAFs such as PAF-18-OH (2.5 mmol g^{-1}), PAF-32-OH (2.3 mmol g^{-1}) and PAF-34-OH (2.2 mmol g^{-1}). Only PAF bearing amino groups overcome the **co-CXF3-OH** performance.[35] Furthermore, CO_2 isosteric heat of adsorption Q_{st} at low coverage is 30 kJ mol^{-1} (Figure 4i), which is significantly higher than 15.6 kJ mol^{-1} determined for PAF-1 and hydroxy functionalized PAF (PAF-1-CH_2OH, 19.3 kJ mol^{-1})[33,40], and matches the values obtained with PAF decorated with polar groups such as F-PAF1 (26 kJ mol^{-1}).[41]

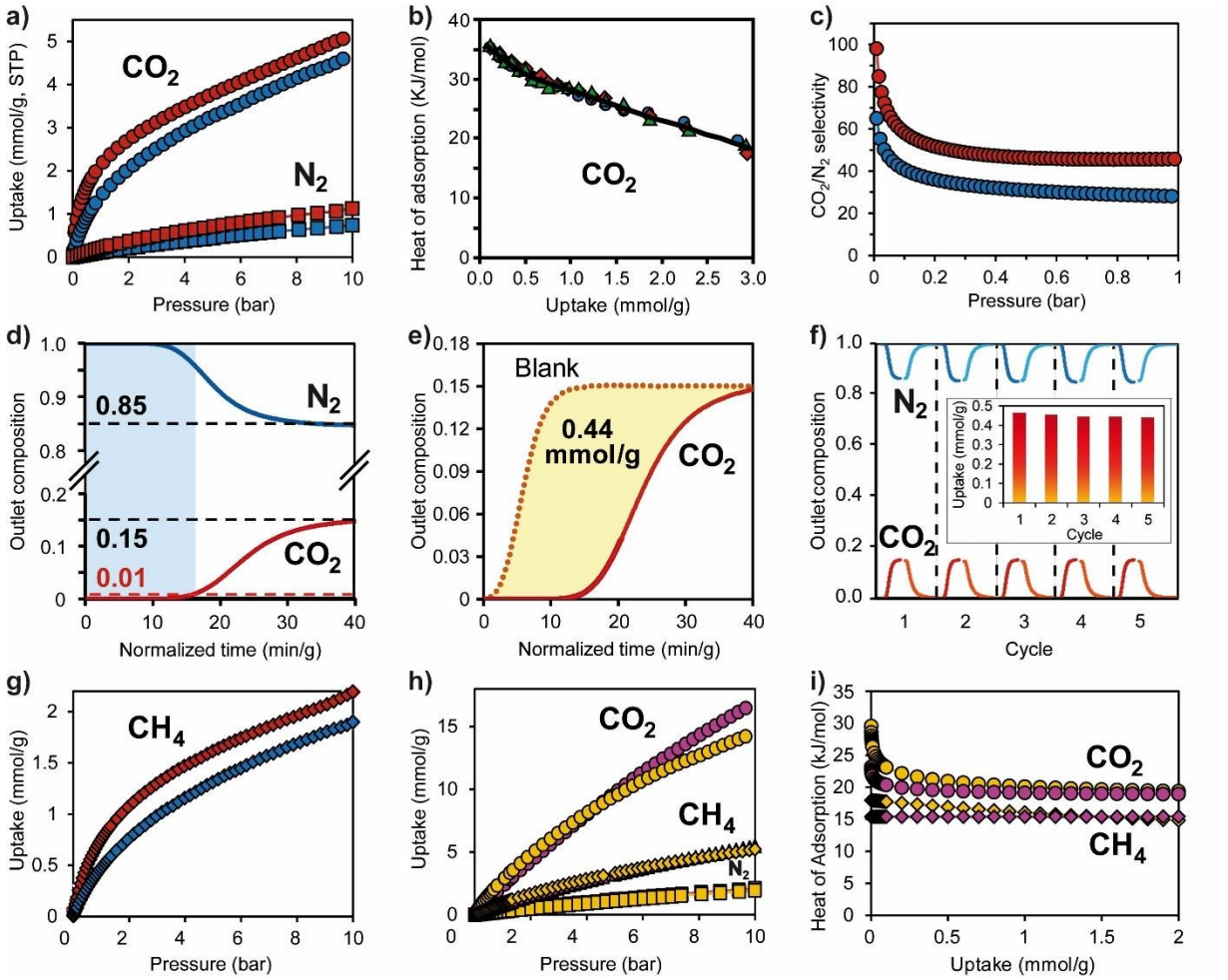

Figure 4. a) CO_2 (circles) and N_2 (squares) adsorption isotherms collected at 273 K and up to 10 bar of **CXF1-OMe** and **CXF1-OH** (blue and red colors, respectively). b) Heat of adsorption of **CXF1-OMe** form microcalorimetry coupled to adsorption apparatus. The three distinct runs show the reproducibility of the measurements. c) CO_2 over N_2 selectivity at 273 K for **CXF1-OH** calculated applying IAST theory to a 15:85 CO_2/N_2 mixture. d) CO_2/N_2 (15/85) breakthrough curves measured with a total flow rate of 4 sccm on **CXF1-OH** sample. e) CO_2 breakthrough curves compared with blank response: the yellow shaded area was integrated to calculate the total amount of CO_2 adsorbed under dynamic conditions. The uptake of 0.44 mmol/g is in agreement with the pure CO_2 adsorption under same partial pressure and temperature conditions (0.45 mmol/g). f) Breakthrough experiments repeated for five cycles. The desorption was carried out by N_2 flow at room temperature. Column efficiency is constant over all cycles. g) CH_4 adsorption isotherms at 273 K of **CXF1-OMe** and **CXF1-OH** (blue and red diamonds, respectively). h) CO_2, CH_4 and N_2 of **co-CXF3-OPr** and **co-CXF3-OH** at 273 K and up to 10 bar (violet and yellow, respectively). f) Heat of adsorption of CO_2 (circles) and CH_4 (diamonds) of **co-CXF3-OPr** and **co-CXF3-OH** (violet and yellow colors, respectively).

This result is particularly relevant if we consider that only 20 mol % of the framework is constituted by calix[4]arene monomers. A similar trend was observed for CH_4 binding energy (Figure 4i), that increased from 15.4 kJ mol^{-1} to 18.0 kJ mol^{-1} from the OPr-bearing

compound to the OH-containing framework. Despite the lower surface area, methane adsorption value at 273 K and 1 bar for **co-CXF3-OH** (1.0 mmol g^{-1}) is higher than that measured for **co-CXF3-OPr** (0.86 mmol g^{-1}), matching the values of PAFs with even higher surface areas.[35]

Conclusions

The preparation of a family of metal-free porous frameworks comprising calixarene moieties stably linked to a 3D framework by covalent bonds is reported. The alkoxy groups on the monomer units were systematically varied to modulate the adsorption properties of gases relevant for energy and pollution issues, such as methane and carbon dioxide. Post synthetic modification of the functionalities to yield polyhydroxy-frameworks were successfully achieved and showed competitive sorption performances. The adsorption energies as high as 35 and 24 kJ mol^{-1} for CO_2 and CH_4, respectively, fall in the proper interval for useful applications in the fields of delivery, capture, purification and storage. CO_2 selective adsorption with respect to N_2 was tested under operative conditions by column breakthrough runs, resulting in nitrogen purification.

Additionally, xenon absorbed in the pores was *in-situ* observed with high sensitivity by hyper-polarization NMR, which could determine the rapid uptake in the accessible galleries to reach calixarene effective sites and xenon confinement in between the aromatic rings. High surface area (3000 m^2 g^{-1}) copolymers of calixarene with tetraphenylmethane monomer units were engineered, which showed the tunability of the method to build structures balanced between high capacity (provided by aromatic units) and gas retention (associated with calixarene units). Also in the case of copolymer, removal of the alkoxy moieties resulted in best-performing nanoporous materials.

The chemical and thermal stability of the networks support the idea that this family of metal-free compounds may well compete with the strive for achieving environmentally useful, moderate costs, scale-up compatible, substances. For the uses, beyond the scope of the present investigation, we wish to mention separation of pollutants from water, since they are recyclable and not hydrolyzed for an indefinite time.

Author Contributions

A.P. and J.P. equally contributed to the synthesis and general characterization, J.P. and C.X.B. collected and discussed gas adsorption, Breakthrough and microcalorimetry data, S.B. performed and analysed NMR spectra. P.S. and A.C. coordinated the project.

Conflicts of interest

There are no conflicts to declare.

View Article Online
DOI: 10.1039/D1TA05930K

Acknowledgements

Financial support from the Italian Ministry of University and Research (MIUR) through the grant 'Dipartimenti di Eccellenza-2017 Materials For Energy' is acknowledged. This research was funded by PRIN-20173L7W8K (NEMO) grant. We would like to thank M. Negroni for technical support.

Notes and references

1 S. Kumar, S. Chawla and M. C. Zou, *J. Incl. Phenom. Macrocycl. Chem.,* 2017, **88**, 129–158.
2 N. B. Mckeown, *J. Mater. Chem.,* 2010, **20**, 10588–10597.
3 P. Sozzani, S. Bracco, A. Comotti, L. Ferretti, R. Simonutti, *Angew. Chem. Int. Ed.,* 2005, **44**, 1816–1820.
4 S. J. Dalgarno, P. K. Thallapally, L. J. Barbour, J. L. Atwood, *Chem. Soc. Rev.*, 2007, **36**, 236-245.
5 J. L. Atwood, L. J. Barbour, P. K. Thallapally, T. B. Wirsig, *Chem. Commun.,* 2005, **51**, 51–53.
6 K. A. Udachin, I. L. Moudrakovski, G. D. Enright, C. I. Ratcliffe, J. Ripmeester, *Phys. Chem. Chem. Phys.,* 2008, **10**, 4636–4643.
7 V. V. Gorbatchuk, A. G. Tsifarkin, I. S. Antipin, B. N. Solomonov, A. I. Konovalov, J. Seidel, F. Baitalov, *J. Chem. Soc. Perkin Trans. 2,* 2000, 2287–2294, doi:10.1039/b003477k.
8 J. Atwood, L. J. Barbour, A. Jerga, B. L. Schottel, *Science*, 2002, **298**, 1000-1002.
9 S. Das, P. Heasman, T. Ben, S. Qiu, *Chem. Rev.,* 2017, **117**, 3, 1515–1563.
10 J. S. M. Lee, A. I. Cooper, *Chem. Rev.,* 2020, **120**, 2171–2214.
11 A. Giri, A. Sahoo, T. K. Dutta, A. Patra, *ACS Omega,* 2020, **5**, 28413-28424.
12 O. Buyukcakir, Y. Seo, A. Coskun, *Chem. Mater.,* 2015, **27**, 4149−4155.
13 A. Alsbaiee, B. J. Smith, L. Xiao, Y. Ling, D. E. Helbling, W. R. Dichtel, *Nature,* 2016, **529**, 190−194.
14 Y. Zhang, J. Duan, D. Ma, P. Li, S. Li, H. Li, J. Zhou, X. Ma, X. Feng, B. Wang, *Angew. Chem. Int. Ed.,* 2017, **56**, 16313−16317.
15 S. N. Talapaneni, D. Kim, G. Barin, O. Buyukcakir, S. H. Je, *Chem. Mater.,* 2016, **28**, 4460–4466.
16 K.Su, W. Wang, B. Li, D. Yuan, *ACS Sustain. Chem. Eng.,* 2018, **6**, 17402–17409.
17 A. Giri, M. W. Hussain, B. Sk, A. Patra, *Chem. Mater.,* 2019, **31**, 8440–8450.
18 D. Shetty, J. Raya, D. S. Han, Z. Asfari, J. C. Olsen, A. Trabolsi, *Chem. Mater.,* 2017, **29**, 8968–8972.
19 D. Shetty, I. Jahovic, J. Raya, F. Ravaux, M. Jouiad, J. C. Olsen, A. Trabolsi, *J. Mater. Chem. A,* 2017, **5**, 62–66.
20 D. Shetty, I. Jahovic, J. Raya, Z. Asfari, J. C. Olsen, A. Trabolsi, *ACS Appl. Mater. Interfaces,* 2018, **10**, 2976–2981.
21 D. M. Roundhill, Calixarenes. In *Comprehensive Coordination Chemistry II*; Monographs in Supramolecular Chemistry; Royal Society of Chemistry: Cambridge, 2004; Vol. 1, pp. 485–491.
22 A. Arduini, A. Casnati, Calixarenes. In *Macrocycle Synthesis: A Practical Approach*; Parker, D., Ed.; 1996; pp. 145–173.
23 C. D. Gutsche, Shaping the baskets: Conformations of calixarenes. In *Calixarenes Revisited*; 2007; pp. 41–78.
24 A. Casnati, J. de Mondoza, D. N. Reinhout, D. Ungaro, In *NMR in Supramolecular Chemistry*; Pones, M. Ed.; 1999; pp. 307-310.
25 T. Ben, H. Ren, M. Shengqian, D. Cao, J. Lan, X. Jing, W. Wang, J. Xu, F. Deng, J. M. Simmons, S. Qiu, G. Zhu, *Angew. Chem. Int. Ed.,* 2009, **48**, 9457–9460.
26 V. L. Furer, E. I. Borisoglebskaya, V. I. Kovalenko, *Spectrochim. Acta - Part A Mol. Biomol. Spectrosc.,* 2005, **61**, 355–359.
27 V. Böhmer, *Angew. Chem. Int. Ed.* 1995, **34**, 713-745.

View Article Online
DOI: 10.1039/D1TA05930K

28 A. Comotti, S. Bracco, L. Ferretti, M. Mauri, R. Simonutti, P. Sozzani, *Chem. Comm.,* 2007, 350-352.
29 A. Comotti, S. Bracco, P. Sozzani, S. Horike, R. Matsuda, J. Chen, M. Takata, Y. Kubota, S. Kitagawa, *J. Am. Chem. Soc.,* 2008, **130**, 13664-13672.
30 R. Simonutti, S. Bracco, A. Comotti, M. Mauri, P. Sozzani, *Chem. Mater.,* 2006, **18,** 4651-4657.
31 P. Sozzani, S. Bracco, A. Comotti, M. Mauri, R. Simonutti, P. Valsesia, *Chem. Comm.,* 2006, 1921-1923.
32 W. K. Feldmann, K.-A. White, C. X. Bezuidenhout, V. J. Smith, C. Esterhuysen, L. J. Barbour, *ChemSusChem*, 2020, **13** 102-105.
33 S. J. Garibay, M. H. Weston, J. E. Mondloch, Y. J. Colón, O. K. Farha, J. T. Hupp, S. T. Nguyen, *Cryst. Eng. Comm.,* 2013, **15**, 1515–1519.
34 J. Perego, D. Piga, S. Bracco, P. Sozzani, A. Comotti, *Chem. Commun.,* 2018, **54**, 9321–9324, doi:10.1039/C8CC03951H.
35 Y. Tian, G. Zhu, *Chem. Rev.,* 2020, **120**, 8934–8986.
36 W. Liang, P. M. Bhatt, A. Shkurenko, K. Adil, G. Mouchaham, H. Aggarwal, A. Mallick, A. Jamal, Y. Belmabkhout, and M. Eddaoudi, *Chem*., 2019, **5**, 950–963.
37 S. H. Je, O. Buyukcakir, D. Kim, A. Coskun, *Chem.* 2016, 1, 482-493.
38 Y. Peng, V. Krungleviciute, I. Eryazici, J. T. Hupp, O. K. Farha, T. Yildirim, *J. Am. Chem. Soc.,* 2013, **135**, 11887–11894.
39 J. L. Mendoza-Cortes, T. A. Pascal, W. A. Goddard, W. A. *J. Phys. Chem. A,* 2011, **115**, 13852–13857.
40 T. Ben, C. Pei, D. Zhang, J. Xu, F. Deng, X. Jing, S. Qiu, *Energy Environ. Sci.,* 2011, **4**, 3991–3999, doi:10.1039/c1ee01222c.
41 A. Comotti, F. Castiglioni, S. Bracco, J. Perego, A. Pedrini, *Chem. Commun.,* 2019, **55**, 8999–9002.